Performance of Max-Ortho Basis Functions in FEM Scattering Analysis

Slobodan V. Savić, *Member, IEEE*, Milan M. Ilić, *Senior Member, IEEE*,
and Branko M. Kolundzija, *Fellow, IEEE*

Abstract—**Performance of previously developed maximally orthogonalized higher order basis functions implemented in the large-domain finite element method are additionally evaluated in two numerical examples. In our previous work these basis functions were used only for non-radiating problems. In order to expand their scope, and make them suitable for radiating problems also, in this work these basis functions are combined with the first order absorbing boundary condition. It is shown that this does not degrade their superiority regarding the condition number.**

Index Terms—**Condition number; finite element method; higher-order basis functions; higher-order modeling; numerical analysis; orthogonal functions.**

I. INTRODUCTION

TWO most popular numerical techniques for solving general linear electromagnetic (EM) problems in the frequency domain are the finite element method (FEM) [1, 2] and the method of moments (MoM) [3, 4]. After expanding EM quantities in terms of basis functions and unknown coefficients, the final system of linear equations must be solved, which can represent a significant percentage of the total simulation execution time. There are several algorithms for solving systems of linear equations (iterative methods being some of them). In any case, larger systems of equations require more computational recourses and more time to be solved.

It is generally accepted that div- and curl-conforming higher-order basis functions are more efficient then low-order functions [5, 6], i.e., that they yield a smaller system of linear equations for the same accuracy, compared to low-order basis functions. Unfortunately, in their original form, hierarchical higher-order basis functions possess significant linear dependence, which leads to ill-conditioned system-matrices. This, in turn, limits the maximal order of basis functions in the mesh [7], and disables the efficient usage of iterative solvers [8, 9].

Great amount of work has been done within the community in attempts to construct more orthogonal and linearly independent basis functions [10-14]. In [15] a general theory

S. V. Savić is with the School of Electrical Engineering, University of Belgrade, Serbia (phone: +381 11 3218 351; e-mail: ssavic@etf.bg.ac.rs).

M. M. Ilić is with the School of Electrical Engineering, University of Belgrade, Serbia (e-mail: milanilic@etf.bg.ac.rs).

B. M. Kolundzija is with the School of Electrical Engineering, University of Belgrade, Serbia (e-mail: kol@etf.bg.ac.rs).

of maximally orthogonal div- and curl-conforming higher-order basis functions is presented for generalized wires, quadrilaterals and hexahedra. Explicit expressions for these basis functions are presented up to the eight order and numerical results are presented for the MoM-SIE. In [16] maximally orthogonal basis functions where implemented in the higher-order large-domain FEM, and the novel two-term recurrent formulas for their calculation were developed.

As a continuation of our work in [9], [15] and [16], here we evaluate the accuracy and orthogonality of the maximally orthogonal basis functions in the higher-order large-domain FEM in two numerical experiments. As an addition to the numerical experiments from [16], these examples cover problems frequently encountered in engineering practice.

The rest of this paper is organized as follows. To keep the paper self-contained, the relevant theory of the higher order large-domain FEs is given in Section II. Three types of basis functions (classical, near-ortho and max-ortho), used in the higher-order FEM, are presented in Section III. Results of numerical experiments are presented in Section IV, and the concluding remarks are given in Section V.

II. HIGHER ORDER LARGE-DOMAIN FINITE-ELEMENT TECHNIQUE

As a basic element for the geometrical modeling of arbitrary shaped 3-D electromagnetic (EM) structures in the FEM, we use a generalized curved parametric hexahedron [6] whose geometry is defined as

$$\mathbf{r}(u,v,w) = \sum_{m=0}^{K_u}\sum_{n=0}^{K_v}\sum_{l=0}^{K_w}\mathbf{r}_{mnl}L_m^{K_u}(u)L_n^{K_v}(v)L_l^{K_w}(w), \quad (1)$$
$$-1 \le u,v,w \le 1,$$

where $\mathbf{r}_{mnl}$ are the position vectors of the interpolation nodes, K_u, K_v, and K_w are the geometrical orders of the element along u-, v- and w-parametric coordinates, and $L_m^{K_u}$, $L_n^{K_v}$, and $L_l^{K_w}$ are the Lagrange interpolating polynomials [6]. Equation (1) defines a mapping from a cubical parent domain ($-1 \le u,v,w \le 1$) to the generalized hexahedron, as illustrated in Fig. 1. All parameters of a FE, such as its basis functions, are defined in the parent domain and mapped through (1) to the global domain, i.e., to the *xyz*-coordinate system in Fig. 1.

In the FEM formulation, we start from the curl-curl electric field vector-wave equation [6]

$$\nabla \times \mu_r^{-1}\nabla \times \mathbf{E} - k_0^2\varepsilon_r\mathbf{E} = 0, \quad (2)$$

where ε_r and μ_r are complex relative permittivity and permeability of the medium, $\mathbf{E}$ is the electric-field complex intensity vector, $k_0 = \omega\sqrt{\varepsilon_0\mu_0}$ is the free-space wave number, ε_0 and μ_0 are permittivity and permeability of free space, and ω is the angular frequency of the implied time-harmonic excitation. Inside each element we approximate the electric-field intensity vector as

$$\mathbf{E} = \sum_{i=0}^{N_u-1}\sum_{j=0}^{N_v}\sum_{k=0}^{N_w}\alpha_{uijk}\mathbf{f}_{uijk} + \sum_{i=0}^{N_u}\sum_{j=0}^{N_v-1}\sum_{k=0}^{N_w}\alpha_{vijk}\mathbf{f}_{vijk} + \sum_{i=0}^{N_u}\sum_{j=0}^{N_v}\sum_{k=0}^{N_w-1}\alpha_{wijk}\mathbf{f}_{wijk}, \quad (3)$$

where $\mathbf{f}_{uijk}$, $\mathbf{f}_{vijk}$, and $\mathbf{f}_{wijk}$ are the curl-conforming vector basis functions, N_u, N_v, and N_w are adopted orders of the electric field expansion, and α_{uijk}, α_{vijk}, and α_{wijk} are unknown field-distribution coefficients to be determined by the FEM [6].
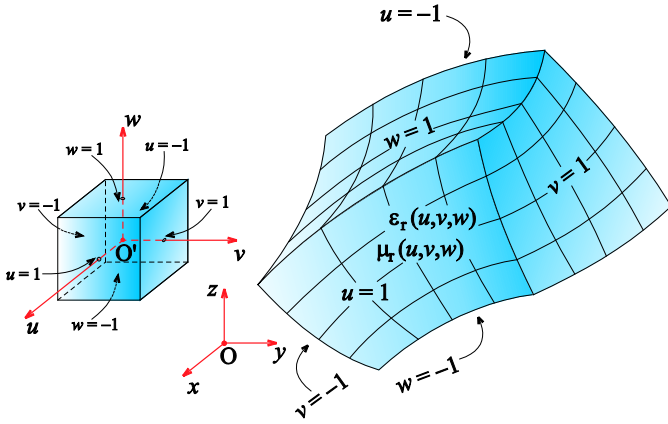
Fig. 1. Cube to hexahedron mapping defined by (1).

A standard Galerkin-type weak-form discretization of (2) yields [9]

$$\int_V \mu_r^{-1}\left(\nabla\times\mathbf{f}_{\tilde{i}\tilde{j}\hat{k}}\right)\cdot\left(\nabla\times\mathbf{E}\right)\mathrm{d}V - k_0^2\int_V \varepsilon_r\mathbf{f}_{\tilde{i}\tilde{j}\hat{k}}\cdot\mathbf{E}\mathrm{d}V =$$
$$= -\oint_S \mu_r^{-1}\mathbf{f}_{\tilde{i}\tilde{j}\hat{k}}\cdot\mathbf{n}\times\left(\nabla\times\mathbf{E}\right)\mathrm{d}S, \quad (4)$$

where V is the volume of the element, $\mathbf{f}_{\tilde{i}\tilde{j}\hat{k}}$ stands for any of the testing functions, S is the surface of the element, and $\mathbf{n}$ is the outward unit normal to the surface of the element. (In the Galerkin method, testing functions are the same as the basis functions.) Electric field expansion from (3) is substituted in (4), leading to the final system of linear equations with unknown coefficients α_{uijk}, α_{vijk} and α_{wijk}. In the final discretized form of (4) the first integral on the left-hand side produces the entries of the FEM stiffness matrix, whereas the second integral produces the entries of the FEM mass matrix [1].

In the higher-order finite-element technique we use, basis functions are constructed from polynomials [6]. For the same field-expansion orders [N_u, N_v, and N_w in (3)], namely for the same degree of polynomial approximation of the EM field distribution, these polynomials can be arranged in different ways and different polynomials can be assigned to different basis functions [16]. Regardless of the way in which the polynomials are arranged, they span the same space and they equivalently approximate the EM field. On the other hand, they result in different stiffness and mass matrices and they produce different systems of linear equations. Because of this, by starting from one arrangement of polynomials in original basis functions, we can rearrange them in order to get the system of linear equations best suited for solving by standard numerical procedures. The condition number of the matrix is one of the parameters describing the corresponding system of equations in this sense, and, generally, matrices with smaller condition number are preferable, i.e., yield numerically more stable solutions.

III. BASIS FUNCTIONS AND THEIR ORTHOGONALITY IN THE HIGHER ORDER FEM

The curl-conforming basis functions can be represented as [6]

$$\mathbf{f}_{uijk} = P_i(u)S_j(v)S_k(w)\mathbf{a}^u,$$
$$\mathbf{f}_{vijk} = S_i(u)P_j(v)S_k(w)\mathbf{a}^v, \quad (5)$$
$$\mathbf{f}_{wijk} = S_i(u)S_j(v)P_k(w)\mathbf{a}^w,$$

where $\mathbf{a}^u$, $\mathbf{a}^v$ and $\mathbf{a}^w$ are reciprocal unitary vectors defined as

$$\mathbf{a}^u = \mathbf{a}_v\times\mathbf{a}_w/J, \quad \mathbf{a}^v = \mathbf{a}_w\times\mathbf{a}_u/J, \quad \mathbf{a}^w = \mathbf{a}_u\times\mathbf{a}_v/J, \quad (6)$$

J is the Jacobian of the covariant transformation

$$J = \left(\mathbf{a}_u\times\mathbf{a}_v\right)\cdot\mathbf{a}_w, \quad (7)$$

and $\mathbf{a}_u$, $\mathbf{a}_v$ and $\mathbf{a}_w$ are unitary vectors defined as

$$\mathbf{a}_u = \mathrm{d}\mathbf{r}/\mathrm{d}u, \quad \mathbf{a}_v = \mathrm{d}\mathbf{r}/\mathrm{d}v \quad \text{and} \quad \mathbf{a}_w = \mathrm{d}\mathbf{r}/\mathrm{d}w, \quad (8)$$

with $\mathbf{r}$ given in (1).

Two basis functions $\mathbf{f}_i$ and $\mathbf{f}_j$ are said to be orthogonal if their inner product is equal to zero [15, 16], i.e., if

$$\left\langle\mathbf{f}_i,\mathbf{f}_j\right\rangle = \int_V \mathbf{f}_i\cdot\mathbf{f}_j\,\mathrm{d}V = 0, \quad i\neq j, \quad (9)$$

where V is the volume of the particular FE. Based on (9), basis functions belonging to different elements are inherently mutually orthogonal.

The orthogonality condition (9) takes into account the polynomial form of the basis functions, but also the geometry of the particular element [through the unitary and reciprocal unitary vectors, as well as the Jacobian appearing in (5) and (6)]. The orthogonality condition defined this way is very restrictive, so it is very challenging to develop basis functions orthogonal in this sense for a general (curved) FE. Because of this, we will consider less general and less restrictive orthogonality condition in which it is assumed that a FE has mutually orthogonal coordinate lines with constant unitary and reciprocal unitary vectors. In this particular case, the basis functions orthogonality defined in (9) can be reduced to the orthogonality of P- and S-functions from (5) [15, 16]. We will thus consider the two basis functions to be mutually

orthogonal if their *P*- and *S*-functions satisfy

$$\langle P_i, P_j \rangle = \int_{u=-1}^{1} P_i(u) P_j(u) du = 0 , \ i \neq j , \ \text{and} \qquad (10)$$

$$\langle S_i, S_j \rangle = \int_{u=-1}^{1} S_i(u) S_j(u) du = 0 , \ i \neq j . \qquad (11)$$

Based on this we can define the orthogonality factors for *P*- and *S*-functions as [15, 16]

$$o_{ij}^P = \frac{\langle P_i, P_j \rangle}{\sqrt{\langle P_i, P_i \rangle}\sqrt{\langle P_j, P_j \rangle}} \ \text{and} \ o_{ij}^S = \frac{\langle S_i, S_j \rangle}{\sqrt{\langle S_i, S_i \rangle}\sqrt{\langle S_j, S_j \rangle}} . (12)$$

Next, we consider three types of basis functions and their orthogonality: classical basis functions (CLBFs), near-ortho basis functions (NOBFs), and max-ortho basis functions (MOBFs), and we examine their performance and behavior in the context of the higher order large-domain FEM.

For CLBFs, *P*- and *S*-functions [in (5)] are defined as [5, 6, 15, 16]

$$P_i(u) = u^i,$$

$$S_j(v) = \begin{cases} 1 - (-1)^j v, & j = 0,1 \\ v^j - 1, & j = 2, 4, 6, ... \\ v^j - v, & j = 3, 5, 7, ... \end{cases} , \ -1 \leq u, v \leq 1. \qquad (13)$$

S-functions (S_j , $j \geq 0$) can be divided into two groups: S_0 and S_1 will be called *node S-functions*, and S_j , $j \geq 2$, will be called *segment S-functions*, as in [15, 16]. Only basis functions with appropriate node *S*-functions establish the continuity of the tangential component of the electric field at a face shared by adjacent elements, making them curl-conforming.

For near-ortho basis functions, *P*- and *S*-functions are defined as [9, 11, 15]

$$P_i(u) = L_i(u),$$

$$S_j(v) = \begin{cases} L_0(v) - (-1)^j L_1(v), & j = 0,1 \\ L_j(v) - L_{j-2}(v), & j \geq 2 \end{cases} , \ -1 \leq u, v \leq 1, \qquad (14)$$

where L_i are Legendre polynomials of order i .

Max-ortho segment *S*-functions, S_j , $j \geq 2$, can be constructed in the form [15, 16]

$$S_j(v) = L_j(v) - L_{j-2}(v) + D_j S_{j-2}(v) , \quad j \geq 2, \qquad (15)$$

and recurrent formula for the unknown coefficients D_j is derived in [16]

$$D_2 = 0, \ D_3 = 0, \ D_j = \frac{2j-7}{4j-10-(2j-3)D_{j-2}} , \ j \geq 4 .(16)$$

Max-ortho node *S*-functions, S_0 and S_1 , can be constructed in the form [15, 16]

$$S_j^N(v) = L_0(v) - (-1)^j L_1(v) + \sum_{k=2}^{N} D_j^k S_k(v) , \quad j = 0,1, \qquad (17)$$

where N is an appropriate field-expansion order and S_k , $2 \leq k \leq N$ are max-ortho segment *S*-functions from (15). The

recurrent formula for the unknown coefficients D_0^k and D_1^k , $2 \leq k \leq N$, is determined in [16]

$$D_j^0 = 1, \ D_j^1 = (-1)^{j+1}, \ D_j^k = \frac{2k+1}{2k-3} D_j^{k-2} D_{k+2}, \ \begin{matrix} j = 0,1 \\ 2 \leq k \leq N \end{matrix} .(18)$$

Notice that the max-ortho node *S*-functions are not mutually orthogonal, and that they are not hierarchical. The fact that these functions are not hierarchical has different practical implications in the FEM and the MoM-SIE, and this will be the subject of our future research. Additionally, in [17] it is shown that high-order Legendre polynomials and their derivatives cannot be calculated precisely simply by linearly combining power functions, and that they should be calculated recurrently. Thus, the max-ortho basis functions should also be calculated recurrently (as they contain Legendre polynomials in our implementation). Based on this, the recurrent formulas (16) and (18) are perfectly suited for efficient and precise calculation of the max-ortho basis functions.
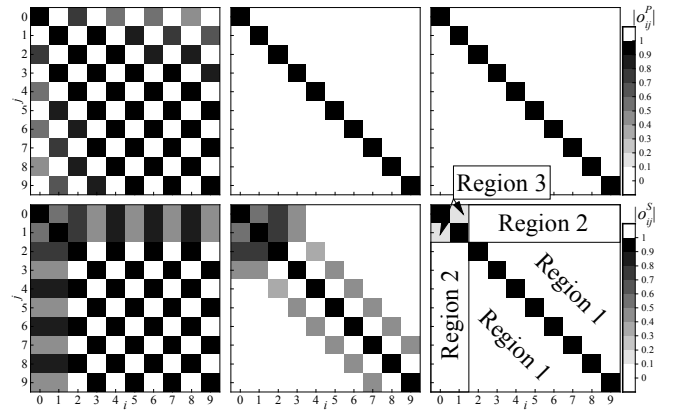
Fig. 2. Matrix form of orthogonality factors | o_{ij}^P | (top row) and | o_{ij}^S | (bottom row) for (a) classical, (b) near-ortho and (c) max-ortho basis functions.

Absolute values of orthogonality factors o_{ij}^P and o_{ij}^S are plotted in Fig. 2 in the form of a matrix for CLBFs, NOBFs and MOBFs up to the ninth order ($0 \leq i,j \leq 9$), similarly as in [15, 16]. For CLBFs, the matrices of the orthogonality factors o_{ij}^P and o_{ij}^S [Fig. 2 (a)] have many non-zero elements, thus the majority of basis functions are not mutually orthogonal. For NOBFs, *P*-functions are completely mutually orthogonal and the matrix of the orthogonality factors o_{ij}^P is an identity matrix [Fig. 2(b)]. *S*-functions are not completely mutually orthogonal, but, when compared with CLBFs, the matrix of the orthogonality factors o_{ij}^S is sparser. Finally, as it can be seen from Fig. 2(c), max-ortho *P*-functions are completely mutually orthogonal, segment *S*-functions are completely mutually orthogonal (Region 1), node *S*-functions are completely orthogonal to the segment *S*-functions, (Region 2), node *S*-functions are not mutually orthogonal (Region 3), and the matrix of the orthogonality factors o_{ij}^S is the sparsest for the MOBFs. Based on these results, it seems reasonable to

assume that the MOBFs will lead to the smallest condition number of the FEM mass matrix, especially when the mesh consists of electrically large elements with high field-expansion orders.

IV. NUMERICAL EXAMPLES

In this section we examine the performance of MOBFs implemented in higher order large-domain FEM technique [6]. We also compare their performance with CLBFs and NOBFs, similarly as in [16]. In all numerical examples, the entries of the mass and stiffness matrices are diagonally normalized [15] by the entries on the main diagonal of the mass matrix and all real and complex numbers are represented in double-precision floating-point format.

As the first example, consider a spherical perfect electric conductor (PEC) scatterer of radius $a = 1\,\text{m}$, situated in free space. The scatterer is modeled with six second-order ($K = 2$) truncated square pyramid like elements, as shown in the inset of Fig. 3. These elements have inner radius $a = 1\,\text{m}$ and outer radius $b = 1.5\,\text{m}$ with the PEC boundary condition and first-order absorbing boundary condition (ABC) [18] applied to their faces that sit on the scatterer and outer surface, respectively. The scatterer is illuminated by a uniform plane wave. A bistatic radar cross-section (RCS) is calculated at frequency $f \approx 300\,\text{MHz}$ ($\lambda_0 = 1\,\text{m}$ being the corresponding wavelength in a free space). For all elements in the mesh, the field-expansion orders in all directions are set to be equal ($N_u = N_v = N_w = N$).

When solving an EM eigenvalue problem (e.g., as in first two examples from [16]), FEM mass and stiffness matrices are kept separately, and a separate condition number can be calculated for each of them. In contrast with this, when solving radiation or scattering problems, FEM mass and stiffness matrices are combined, resulting in a final FEM matrix. As can be seen from Section II, computation of entries in the stiffness matrix includes the curl operator. The curl operator affects the basis functions, and mutually orthogonal basis functions generally are not mutually orthogonal after the curl operator has been applied. This will definitely degrade the orthogonality of the final FEM matrix compared to the orthogonality of the mass matrix. Nevertheless, it is reasonable to expect that max-ortho basis functions will lead to reduction of the condition number of the final FEM matrix compared to all the other types of basis functions.

Fig. 3 shows the condition number of the normalized final FEM matrix for the spherical scatterer. The results for all three types of basis functions are compared. We can see from Fig. 3 that the MOBFs indeed produce the lowest condition number. When the CLBFs are used, the condition number increases rapidly, and it is expected that after reaching a peak, it will remain practically constant, similarly as in [16].

Fig. 4 shows the normalized L^2 error norm of the computed bistatic RCS [19] for the PEC spherical scatterer. In this example, all three types of basis functions yield similar accuracy in computation of the RCS. One of the main

advantages of the max-ortho basis functions in this example would be the smallest condition number, which is a feature highly sought by the iterative solvers [16].
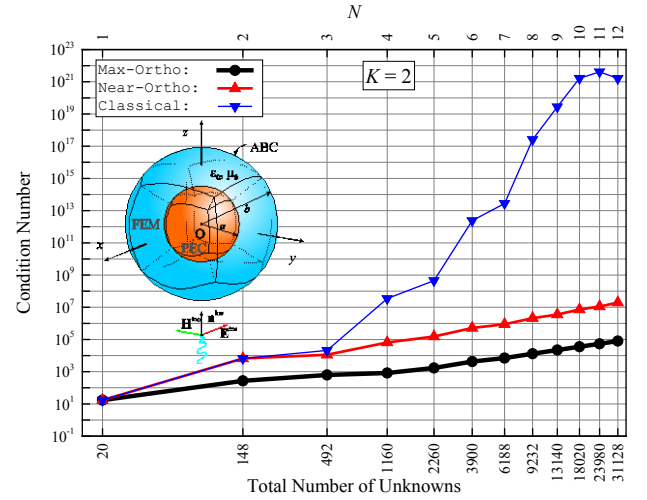
Fig. 3. Condition number of the final FEM matrix for the PEC spherical scatterer; comparison of MOBFs, NOBFs, and CLBFs.
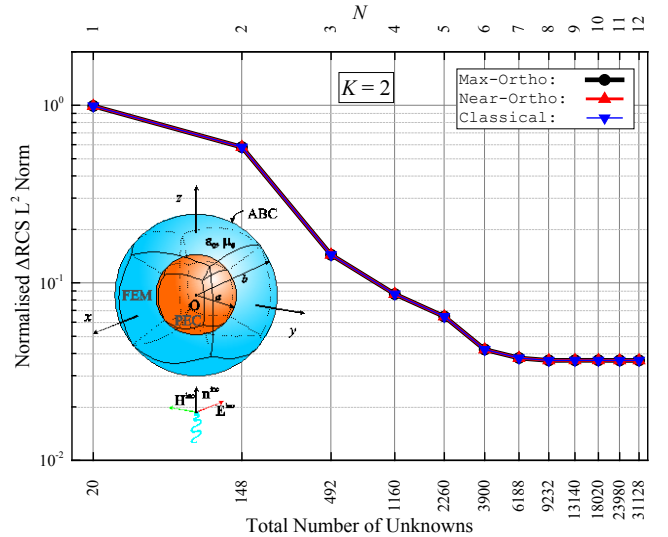
Fig. 4. Normalized L^2 error norm for the computed bistatic RCS of the PEC spherical scatterer; comparison of MOBFs, NOBFs, and CLBFs.

As the second example, consider a waveguide band-pass filter, frequently encountered in engineering practice. The filter consists of an air-filled rectangular PEC waveguide with two PEC stubs in the form of rectangular cuboids. The waveguide is $c = 50\,\text{mm}$ long with dimensions $a = 20\,\text{mm}$ and $b = 10\,\text{mm}$ in the cross-section, as shown in the inset of Fig. 5. The two stubs have a square cross-section, $a_0 = 2\,\text{mm}$ on a side, and they are set symmetrically in the waveguide. Their axes are separated by $c_0 = 17.5\,\text{mm}$.

The filter is meshed with eight trilinear ($K = 1$) elements. For all elements in the mesh, the field-expansion orders in all directions are equal and set to N ($N_u = N_v = N_w = N$).

Fig. 5 shows the condition number of the final FEM matrix

for all three types of basis functions. We can conclude based on this figure that with *p*-refinement [6], the CLBFs lead to a drastic increase of the condition number. On the other hand, the MOBFs have the lowest condition number, whereas the difference in the condition number between the MOBFs and NOBFs is not very large.
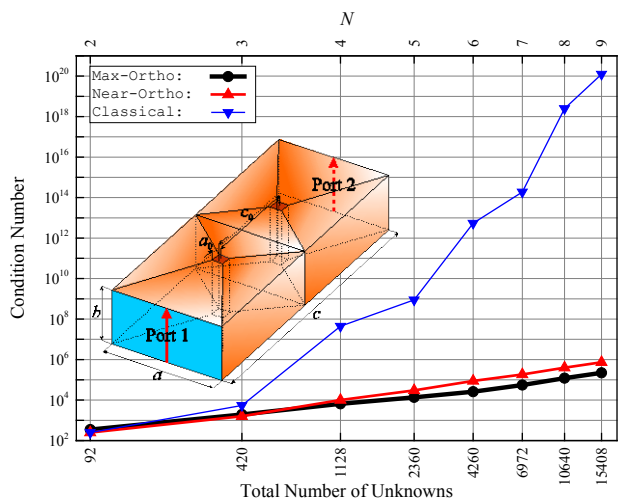
Fig. 5. Condition number of the final FEM matrix for the waveguide band-pass filter; comparison of MOBFs, NOBFs, and CLBFs.
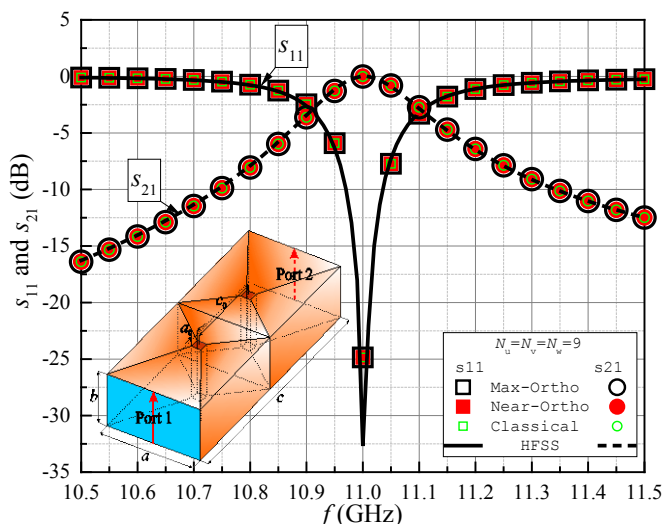
Fig. 6. Scattering parameters of the waveguide band-pass filter; comparison of results obtained by HFSS and by the higher order FEM using MOBFs, NOBFs, and CLBFs.

In order to evaluate the accuracy of the higher-order FEM analysis of the filter and validate the obtained results, we employ a HFSS [20] model for comparison. Fig. 6 shows the comparison of the scattering parameters (*s*-parameters) of the filter computed by our higher order FEM (for the dominant mode excitation) and by HFSS (a fully converged solution). For the higher order FEM, all three set of results (for CLBFs, NOBFs and MOBFs) are shown and we can see from the figure that the agreement of the results is excellent.

V. CONCLUSION

We evaluated the performance of the max-ortho basis functions in comparison with the classical and near-ortho basis functions using two numerical examples. For the scatterer analysis in open space we combined the max-orho basis functions with the first order absorbing boundary condition. The results show that the max-orho basis functions retain their superiority regarding the condition number. We also showed that the max-ortho basis functions lead to the smallest FEM matrix condition number in a waveguide filter analysis problem, which contains geometrically deformed and electrically small finite elements.

REFERENCES

[1] P. P. Silvester and R. L. Ferrari, *Finite Elements for Electrical Engineers*, 3 ed. New York: Cambridge University Press, 1996.
[2] J.-M. Jin, *The Finite Element Method in Electromagnetics*. Hoboken, New Jersey: John Wiley & Sons, 2014.
[3] R. F. Harrington, *Field Computation by Moment Methods* (IEEE Series on Electromagnetic Wave Theory). New Jersey Wiley-IEEE Press, 1993.
[4] B. D. Popović and B. M. Kolundžija, *Analysis of metallic antennas and scatterers* (IEE Electromagnetic Wave Seried 38). London, United Kingdom: The Institution of Electrical Engineers, 1994.
[5] B. M. Kolundžija, "Electromagnetic Modeling of Composite Metallic and Dielectric Structures," *IEEE Trans. Microw. Theory Techn.,* vol. 47, no. 7, pp. 1021-1032, July 1999.
[6] M. M. Ilić and B. M. Notaroš, "Higher order hierarchical curved hexahedral vector finite elements for electromagnetic modeling," *IEEE Trans. Microw. Theory Techn.,* vol. 51, no. 3, pp. 1026-1033, March 2003.
[7] E. M. Klopf, N. J. Šekeljić, M. M. Ilić, and B. M. Notaroš, "Optimal Modeling Parameters for Higher Order MoM-SIE and FEM-MoM Electromagnetic Simulations," *IEEE Trans. Antennas Propag.,* vol. 60, no. 6, pp. 2790-2801, June 2012.
[8] B. M. Kolundžija and T. K. Sarkar, "Iterative Solvers in Frequency Analysis of Complex Structures Based on MoM Solution of Surface Integral Equations," in *Proceedings of IEEE Antennas and Propagation Society International Symposium (APS)*, Boston, MA, USA, 2001, pp. 588-591.
[9] M. M. Ilić and B. M. Notaroš, "Higher Order Large-Domain Hierarchical FEM Technique for Electromagnetic Modeling Using Legendre Basis Functions on Generalized Hexahedra," *Electromagnetics,* vol. 26, no. 7, pp. 517-529, November 2006.
[10] J. P. Webb, "Hierarchal Vector Basis Functions of Arbitrary Order for Triangular and Tetrahedral Finite Elements," *IEEE Trans. Antennas Propag.,* vol. 47, no. 8, pp. 1244-1253, August 1999.
[11] E. Jørgensen, J. L. Volakis, P. Meincke, and O. Breinbjerg, "Higher Order Hierarchical Legendre Basis Functions for Electromagnetic Modeling," *IEEE Trans. Antennas Propag.,* vol. 52, no. 11, pp. 2985-2995, November 2004.
[12] D. S. Sumic and B. M. Kolundzija, "Efficient Iterative Solution of Surface Integral Equations Based on Maximally Orthogonalized Higher Order Basis Functions," in *Proc. in IEEE Antennas and Propagation Society International Symposium (APS)*, Washington, DC, USA, 2005, pp. 288-291.
[13] B. M. Kolundzija and D. S. Sumic, "Optimal Weights of Basis Functions for Efficient Iterative Solution of Surface Integral Equations," in *Proc. in IEEE Antennas and Propagation Society International Symposium (APS)*, Washington, DC, USA, 2005, pp. 284-287.
[14] A. F. Peterson and R. D. Graglia, "Scale Factors and Matrix Conditioning Associated With Triangular-Cell Hierarchical Vector Basis Functions," *IEEE Antennas Wireless Propag. Lett.,* vol. 9, pp. 40-43, February 2010.

[15] M. M. Kostić and B. M. Kolundžija, "Maximally Orthogonalized Higher Order Bases Over Generalized Wires, Quadrilaterals, and Hexahedra," *IEEE Trans. Antennas Propag.,* vol. 61, no. 6, pp. 3153-3148, June 2013.

[16] S. V. Savić, M. M. Ilić, and B. M. Kolundzija, "Maximally Orthogonalized Higher Order Basis Functions in Large-Domain Finite Element Modeling in Electromagnetics," *IEEE Trans. Antennas Propag.,* vol. 68, no. 8, pp. 6455-6460, August 2020.

[17] A. J. Krneta and B. M. Kolundzija, "Using Ultra-High Expansion Orders of Max-Ortho Basis Functions for Analysis of Axially Symmetric Metallic Antennas," *IEEE Trans. Antennas Propag.,* vol. 66, no. 7, pp. 3696-3699, July 2018.

[18] M. M. Ilić, S. V. Savić, and B. M. Notaroš, "First Order Absorbing Boundary Condition in Large-Domain Finite Element Analysis of Electromagnetic Scatterers," in *Proceedings of 10th International Conference on Telecommunications in Modern Satellite, Cable and Broadcasting Services, TELSIKS 2011*, Niš, Serbia, 2011, vol. 2, pp. 424-427.

[19] S. V. Savić, B. M. Notaroš, and M. M. Ilić, "Accuracy Analysis of the Nonrigorous Second-Order Absorbing Boundary Condition Applied to Large Curved Finite Elements," in *2015 International Conference on Electromagnetics in Advanced Applications (ICEAA)*, Turin, Italy, 2015, pp. 58-61.

[20] ANSYS. ANSYS HFSS 15.0.0. ANSYS, 2014, http://www.ansys.com.